Waves in two-dimensional superparamagnetic dusty plasma liquids

Peter Hartmann and Zoltán Donkó
Institute for Solid State Physics, Wigner Research Centre for Physics, Hungarian Academy of Sciences, H-1525 Budapest, P.O. Box 49, Hungary
and Department of Physics, Boston College, Chestnut Hill, Massachusetts 02467, USA

Marlene Rosenberg
Department of Electrical and Computer Engineering, University of California San Diego, La Jolla California 92093, USA

Gabor J. Kalman
Department of Physics, Boston College, Chestnut Hill, Massachusetts 02467, USA
(Received 22 November 2013; published 4 April 2014)

Wave dispersion relations in the strongly coupled liquid phase of a two-dimensional system of dust grains interacting via both Yukawa and dipole interactions are investigated. The model system comprises a layer of charged superparamagnetic grains in a plasma in an external, uniform magnetic field **B** whose magnitude and direction can be varied. Because the induced magnetic dipole moments of the grains lie along **B**, the interaction between the grains becomes anisotropic as **B** is tilted with respect to the layer. The theoretical approach uses a reformulated quasilocalized charge approximation that can treat dipole interactions, combined with molecular dynamics simulations. The mode dispersion relations are found to depend on the relative strengths of the Yukawa and dipole interactions and the direction of wave propagation in the plane.

DOI: 10.1103/PhysRevE.89.043102 PACS number(s): 52.27.Lw, 52.27.Gr

I. INTRODUCTION

Dusty plasmas are plasmas containing fine solid particulates (dust grains) that get electrically charged in the plasma. Typically, the dust grains interact via a screened Coulomb (Yukawa) interaction, where the screening of the dust charge is due to the background plasma ions and electrons (see recent reviews in, e.g., [1–3]). A new area of research in dusty plasmas is the study of systems of dust grains that interact via both Yukawa and dipole interactions. The types of dipole interactions that have been discussed recently include (i) a magnetic dipole interaction, either between superparamagnetic grains that acquire a magnetic dipole moment along an external magnetic field **B** (e.g., [4–6]), or between ferromagnetic particles with intrinsic magnetic dipole moments [7], and (ii) an electric dipole interaction that can be induced by an external alternating electric field that polarizes the screening cloud around a grain, the so-called electrorheological complex plasma (e.g., [8,9]). Both these types of systems could lead to new types of dusty plasma crystals and liquids whose structure and interparticle spacing could be tuned by external means [4,8].

Recently, we investigated the ground-state configuration of a two-dimensional (2D) lattice of charged superparamagnetic grains in a plasma in an external uniform magnetic field **B** whose magnitude and direction with respect to the layer could be varied [6]. When **B** is normal to the layer, the dipole interaction is repulsive. When **B** is tilted with respect to the layer, the magnetic dipole interaction becomes anisotropic. It also becomes attractive along the projection of **B** in the layer if the angle α between **B** and the layer is smaller than a threshold angle $\alpha_{\rm th}$, while it is repulsive otherwise. Molecular dynamics (MD) simulations showed that the structure could change from hexagonal to almost rectangular depending on α and the strength of the ratio of the magnetic to electrostatic interaction.

In this paper, we investigate wave dispersion in the strongly coupled liquid phase of a 2D system of grains interacting via both Yukawa and magnetic dipole-dipole interactions. We consider the case where the magnetic tilt angle α is larger than a threshold $\alpha_{\rm th}$. In this case, the interaction in the dust monolayer is repulsive and anisotropic for $\alpha \neq 90^\circ$ and would generate a stable equilibrium. Due to this anisotropic nature of the interaction, the wave dispersions depend on the direction of propagation in the plane as well as the relative strengths of the Yukawa and dipole interactions. The attractive effect of ion focusing, which has been considered for dust lattice waves in a one-dimensional string of paramagnetic grains [10], is neglected because we are considering a monolayer of dust.

The theoretical approach uses the quasilocalized charge approximation (QLCA) that was recently reformulated by Golden *et al.* [11–13] to calculate wave dispersion in a 2D layer of dipoles with dipole moments perpendicular to the layer. Paralleling the theoretical analysis we have performed detailed molecular dynamics (MD) simulations of the system. The simulation generates fluctuation spectra, which provide the basis for comparison with the calculated collective mode spectrum. We also extract the pair correlation function from the simulations: this latter is needed as input for the QLCA formalism.

The paper is organized as follows. Section II describes the model system. Section III presents the theoretical approach using the QLCA and discusses the MD simulations. Section IV presents results for the mode dispersion relations. Section V discusses possible experimental parameters, and Sec. VI gives a summary.

II. MODEL SYSTEM

The model system is a 2D layer of charged superparamagnetic dust grains of uniform size and material properties

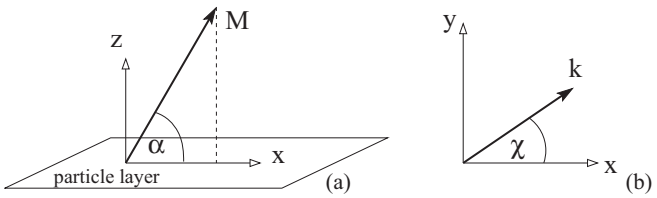

FIG. 1. Geometry of the model system. (a) The dust layer lies in the x-y plane and the magnetic moment $\mathbf{M}$ of each grain lies in the x-z plane at an angle α to the x axis. (b) The angle between the wave vector $\mathbf{k}$ and the x axis is χ.

in a plasma immersed in a constant, homogeneous external magnetic field $\mathbf{B}$. Each grain has a negative electric charge $Q = -Z_d e$ due to plasma collection, where Z_d is the charge state and e is the elementary charge. It is assumed that the grains are strongly coupled in the liquid phase. The $\mathbf{v} \times \mathbf{B}$ motion of the dust is neglected due to the very small charge-to-mass ratio of the dust, which amounts to assuming the dust motion is unmagnetized as, for example, in the case where the dust collision frequency is much larger than the dust gyrofrequency. Owing to their paramagnetic property, each grain acquires a magnetic dipole moment $\mathbf{M}$, which is induced by the external magnetic field and therefore lies in the direction of $\mathbf{B}$. The dust layer lies in the x-y plane, and the magnetic field makes an angle α with respect to the layer. Without loss of generality, we take the x axis to be the direction of the projection of $\mathbf{B}$ in the plane, so that the magnetic moment of each dust grain lies in the x-z plane. We define the direction of wave propagation in the dust layer plane by the angle χ between the wave vector $\mathbf{k}$ and the x axis, as shown in Fig. 1.

The grains interact via an electrostatic screened Coulomb (Yukawa) force and the induced magnetic dipole-dipole force. The electrostatic interaction energy between two grains with charge Q separated by a distance r is

$$\phi_Y = \frac{Q^2}{r} \mathrm{e}^{-\kappa r}, \tag{1}$$

where $\kappa = \lambda_D^{-1}$ is inverse of the plasma Debye screening length. The strength of the effective electrostatic coupling between neighboring grains interacting via this Yukawa potential is generally characterized by the Coulomb coupling parameter $\Gamma = Q^2/ak_BT_d$ and a screening parameter $\bar{\kappa} = a/\lambda_D$. Here $a = (\pi n)^{-1/2}$ is the 2D Wigner-Seitz radius, where n is the areal density of the dust grains, k_B is the Boltzmann constant, and k_BT_d is the thermal (kinetic) energy of the grains. Since it is assumed that the magnetic dipole moments of all the grains are parallel and have the same magnitude, the interaction energy of the two magnetic dipoles is given by [4,14]

$$\phi_M = \frac{M_\mu M_\nu}{r^3}\left(\delta_{\mu\nu} - 3\frac{r_\mu r_\nu}{r^2}\right). \tag{2}$$

We can rewrite (2) noting that $\mathbf{M} \propto \mathbf{B}$, and the component of $\mathbf{B}$ in the plane is $B_\parallel = B\cos\alpha$. Since we have chosen $B_\parallel$ to be in the x direction, the angle between $B_\parallel$ and $\mathbf{r}$ is the polar angle θ. Thus we can write the magnetic dipole interaction as (see also [14])

$$\phi_M = \frac{M^2}{r^3}\,[1 - 3\cos^2\alpha\cos^2\theta]. \tag{3}$$

The electrostatic Yukawa force between the like-charged particles,

$$\mathbf{F}_Y(r) = -\frac{\partial\phi_Y}{\partial r}\hat{\mathbf{r}} = \frac{Q^2}{r^2}(1+\kappa r)e^{-\kappa r}\,\hat{\mathbf{r}}, \tag{4}$$

is always repulsive. In (4), $\hat{\mathbf{r}}$ is a unit vector in the direction of $\mathbf{r}$, which is the vector connecting the two particles. The magnetic dipole-dipole force between the two grains is

$$\begin{aligned}\mathbf{F}_M(r) = -\partial_\mu\phi_M\hat{\mathbf{r}}_\mu = \frac{3M^2}{r^4} \\ \times \{\cos\theta[1 - 5\cos^2\alpha\cos^2\theta + 2\cos^2\alpha]\hat{\mathbf{x}} \\ + \sin\theta[1 - 5\cos^2\alpha\cos^2\theta]\hat{\mathbf{y}}\},\end{aligned} \tag{5}$$

where $\hat{\mathbf{x}}$ and $\hat{\mathbf{y}}$ are unit vectors in the x and y directions, respectively. The magnetic dipole force can be repulsive or attractive depending on the relative positions and orientations of the grains. When $\mathbf{r}$ is purely in the x direction, where the force is softest,

$$F_M(x) = \frac{3M^2}{x^4}(1 - 3\cos^2\alpha), \tag{6}$$

it can be seen that for α smaller than a threshold angle $\alpha_{\mathrm{th}} = \cos^{-1}(1/\sqrt{3}) \approx 54.74^\circ$, the magnetic dipole force becomes purely attractive in this direction. At small distances, the Yukawa interaction goes like $1/r$, while the magnetic dipole interaction potential goes like $1/r^3$. Therefore the magnetic dipole interaction will dominate the Yukawa interaction, and due to thermal fluctuations, agglomeration would ultimately occur [6]. We avoid this scenario in this paper by considering only magnetic tilt angles larger than α_{th}. This corresponds to a stable equilibrium and an interaction, which is repulsive but anisotropic in the dust layer plane for $90^\circ > \alpha > \alpha_{\mathrm{th}}$.

The correlation between dust grains in this system is characterized by an equilibrium pair correlation function $g(r,\theta)$, which is in general a function of r and the polar angle θ (measured from the x axis), with $g(r,\theta) \to 1$ as $r \to \infty$.

III. METHODOLOGY

A. Theoretical approach

The theoretical approach uses the QLCA combined with MD simulations, which has been successfully applied to describe waves in various strongly coupled Yukawa systems in the liquid phase (see review in Ref. [15]), including recently waves in strongly coupled magnetized one-component plasmas [16]. The QLCA is based on the premise that in the strongly coupled liquid phase, the charged particles are quasilocalized, occupying randomly located sites and undergoing small amplitude oscillations around them. It is assumed that the underlying equilibrium configuration, or position of the sites, changes, but on a longer time scale so that one can neglect the diffusion of the quasisites compared to correlational effects (see review in Ref. [17]).

The QLCA was recently reformulated by Golden *et al.* [11–13] to calculate wave dispersion in 2D layer of dipoles with dipole moments perpendicular to the layer. In this system, there is a $1/r^3$ dipole interaction whose spatial integral is divergent. Consequently one has to combine the pair correlation function

with the dipole interaction to obtain an tractable effective potential. Since this reformulated QLCA enables one to treat the dipole interaction, we use this scheme to calculate the wave dispersions in our model system where the dust grains interact via both Yukawa and magnetic dipole-dipole interactions. The details of the derivation of the mode dispersion relations for the isotropic 2D dipole system discussed above are given in Ref. [11]. Here we include an angular dependence in the calculation, and take into account the Yukawa interaction as well by taking the magnetic dipole and Yukawa interactions to be additive.

The mode dispersion relations are given by (see Refs. [11,13])

$$||\omega^2\delta_{\mu\nu} - C_{\mu\nu}(\mathbf{k})|| = 0, \tag{7}$$

where $C_{\mu\nu}(\mathbf{k})$ is the QLCA dynamical matrix,

$$C_{\mu\nu}(\mathbf{k}) = -\frac{n}{m_d}\int d^2r d\theta g(r,\theta)[\exp(i\mathbf{k}\cdot\mathbf{r}) - 1]\partial_\mu\partial_\nu\phi_{\rm Tot}. \tag{8}$$

Here m_d is the dust particle mass, and $\phi_{\rm Tot}$ is the total interaction potential, which is the sum of the Yukawa potential (1) and the magnetic dipole interaction potential (3). For the Yukawa interaction, we have

$$\partial_\mu\partial_\nu\phi_Y = -\frac{Q^2}{r^3}\exp(-\kappa r) \times\left[(1+\kappa r)\left(\delta_{\mu\nu} - 3\frac{r_\mu r_\nu}{r^2}\right) - \frac{r_\mu r_\nu}{r^2}\kappa^2 r^2\right]. \tag{9}$$

For the magnetic dipole-dipole interaction, we have

$$\partial_\mu\partial_\nu\phi_M = -\frac{3M^2}{r^5}\left[(m^2-5d^2)\delta_{\mu\nu} - 5(m^2-7d^2)\frac{r_\mu r_\nu}{r^2} - 10d\left(\frac{m_\mu r_\nu}{r} + \frac{m_\nu r_\mu}{r}\right) + 2m_\mu m_\nu\right]. \tag{10}$$

Here, $\mathbf{m} = [\cos\alpha, 0, \sin\alpha]$, $m^2 = m_\mu m_\mu$, and $d = m_\mu(r_\mu/r) = \cos\alpha\cos\theta$. The physical meaning of the dynamical matrix $C_{\mu\nu}$ can be understood as representing the weighted average of all the forces that act on a particle from its neighbors. It includes two distinct contributions: one is a restoring force due to neighboring particles at their equilibrium sites, which acts when a particle is displaced from its equilibrium position; the other is due to neighboring particles, which have moved from their equilibrium positions and affect the particle to behave in a similar fashion. In this sense it can be regarded as the dynamical equivalent of the elasticity tensor in a solid (see, e.g., Ref. [18]).

Using (9) and (10) we rewrite (8) using the quantities $\bar{r} = r/a$, $\bar{k} = ka$, $\bar{\kappa} = a/\lambda_D$, and $\eta = M/Q\lambda_D$. The quantity η is a measure of the relative magnitude of the magnetic dipole to Yukawa interaction strengths. Further, the angle between $\mathbf{k}$ and $\mathbf{r}$ is given by $(\chi - \theta)$. Then (8) becomes

$$C_{\mu\nu}(\mathbf{k},\alpha,\eta) = \frac{\omega_p^2}{2\pi}\int d\theta\frac{d\bar{r}}{\bar{r}^2}g(\bar{r},\theta)[\exp(i\bar{k}\bar{r}\cos(\chi-\theta)) - 1] \times\left\{\exp(-\bar{\kappa}\bar{r})\left[(1+\bar{\kappa}\bar{r})\left(\delta_{\mu\nu} - 3\frac{\bar{r}_\mu\bar{r}_\nu}{\bar{r}^2}\right) - \frac{\bar{r}_\mu\bar{r}_\nu}{\bar{r}^2}\bar{\kappa}^2\bar{r}^2\right]\right. + \frac{3\eta^2}{\bar{\kappa}^2\bar{r}^2}\left[\left(\delta_{\mu\nu} - 5\frac{\bar{r}_\mu\bar{r}_\nu}{\bar{r}^2}\right) - 5\cos^2\alpha\cos^2\theta\left(\delta_{\mu\nu} - 7\frac{\bar{r}_\mu\bar{r}_\nu}{\bar{r}^2}\right) - 10\cos\alpha\cos\theta\left(m_\mu\frac{\bar{r}_\nu}{r} + m_\nu\frac{\bar{r}_\mu}{\bar{r}}\right) + 2m_\mu m_\nu\right]\Bigg\}. \tag{11}$$

Here $\omega_p = (2\pi Q^2 n/m_d a)^{1/2}$ is the dust plasma frequency in this system.

We will solve (7) using (11) in a Cartesian coordinate system in the x-y plane to obtain the mode dispersions for arbitrary wave number k. The elements of the dynamical matrix $C_{\mu\nu}$ are given explicitly in the Appendix. Since we restrict particle displacements to the x-y plane, we retain only the matrix elements C_{xx}, C_{yy}, C_{xy}, and C_{yx}. The other matrix elements correspond to out-of-plane modes, whose analysis is left for future work. In order to evaluate (11), we need the input of the equilibrium pair correlation function $g(r,\theta)$, which is obtained by MD simulations, described in the next subsection.

Note that for small k, we can expand the exponential factor in (11) in a Taylor series. Because this results in the first nonvanishing term in $C_{\mu\nu}$ being $\propto k^2$, the solution of (7) in this limit yields the phase speeds of the modes.

B. Molecular dynamics simulations

Our molecular dynamics code is an extended version of our earlier code developed for the simulation of Yukawa liquids, see, e.g., Ref. [15]. We simulate the motion of $N = 5000$ particles in the (x,y) plane, within a square box (with a side length of approximately $L = 125\,a$) with periodic boundary conditions, via the integration of their Newtonian equations of motion. The spatial fast decay of the interaction forces makes it possible to introduce a cutoff distance, beyond which the interaction of particle pairs can be neglected when the forces acting on the particles are calculated. For our conditions $r_{\rm cutoff} \approx 30a$. Time integration is performed using the velocity-Verlet scheme. At the initialization of the simulation runs the positions of the particles are set randomly, while their initial velocities are sampled from a Maxwellian distribution corresponding to a specified system temperature. The simulations start with a thermalization phase, during which the particle velocities are rescaled in each time step, in order to reach the desired temperature. This procedure is stopped before the data collection takes place, where the stability of the simulation is confirmed by monitoring the temperature as a function of time. In the measurement phase of the simulation data are collected (i) for the pair correlation function, which becomes spatially anisotropic in the magnetized case, as well as (ii) for the quantities needed for the derivation of the dynamical spectra: the spatial Fourier components of the microscopic density and currents. These are acquired for wave propagation directions at given angles with respect from the direction of the projection of $\mathbf{B}$ on the (x,y) plane. A subsequent Fourier transformation in the time domain [19] yields the dynamical structure functions $S(\mathbf{k},\omega)$,

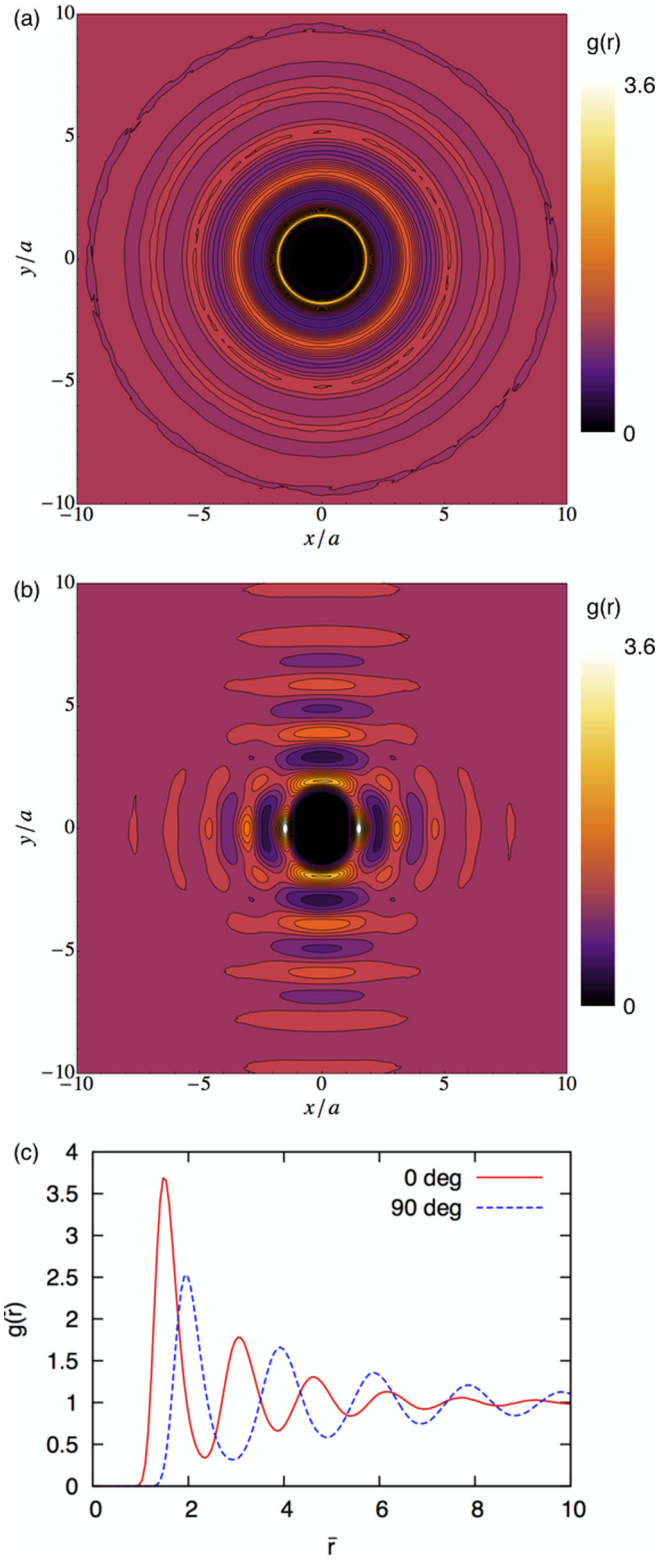

FIG. 2. (Color online) Equilibrium pair correlation function in the dust layer as a function of polar angle θ and $\bar{r}$, for parameters $\bar{\kappa} = 1$, with (a) $\Gamma = 100$ and $\eta = 0$, (b) $\alpha = 60^\circ$, $\Gamma = 25$, and $\eta = 1$. For the parameters in (b), $g(\bar{r})$ is shown in (c) for $\theta = 0^\circ$ (red, solid curve) and $\theta = 90^\circ$ (blue, dashed curve).

as well as the longitudinal and transverse current fluctuation spectra, $L(\mathbf{k},\omega)$ and $T(\mathbf{k},\omega)$, respectively.

IV. NUMERICAL RESULTS

In this section we present the results for the wave dispersion relations using the QLCA, which requires input of the equilibrium pair correlation functions obtained from MD simulations. We also compare the QLCA results with the mode dispersions obtained from the fluctuation spectra generated by the simulations.

Figure 2 shows the equilibrium pair correlation function for a dust layer with $\bar{\kappa} = 1$, and combinations of Γ, η and α (for finite η). Because in our model system the magnetic dipole-dipole interaction is always repulsive, the total effective coupling increases as η increases. When $\eta = 0$ there is no effect of the magnetic field, and the pair correlation function is isotropic in the plane as expected, and is shown in Fig. 2(a). However, for finite η, the total interaction potential is anisotropic in the plane, leading to a rearrangement of the dust particle spacings. Because the strength of the magnetic dipole interaction is largest in the y direction, the dust particle spacing increases in this direction. Since the dust areal density is constant, the dust particles rearrange themselves so that spacings in the x direction decrease somewhat compared to the

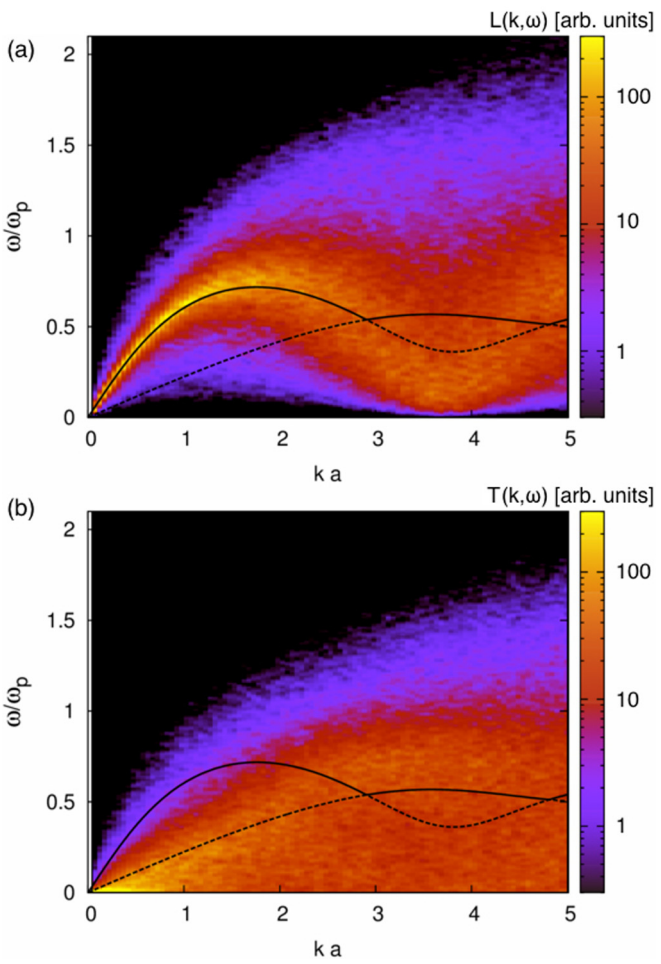

FIG. 3. (Color online) The color maps are the (a) longitudinal and (b) transverse fluctuation spectra generated by the simulations for a Yukawa system with $\Gamma = 100$ and $\bar{\kappa} = 1$. The solid and dashed curves are the QLCA wave dispersion relations for the two modes obtained from Eq. (7) as a function of ka for these parameters.

$\eta = 0$ case. These features can be seen in Figs. 2(b) and 2(c), which show a case with $\Gamma = 25$, $\alpha = 60^\circ$, and $\eta = 1$.

In order to show how the magnetic dipole interaction affects the wave dispersion relations, we first show example dispersion relations for a pure Yukawa system with $\Gamma = 100$ and $\bar{\kappa} = 1$ in Fig. 3. In these figures, the solid and dashed curves are the two QLCA dispersion relations for the two modes obtained from Eq. (7) using (11) and solved in Cartesian coordinates in the x-y plane. These curves are superimposed on the fluctuation spectra generated by the simulations. Figure 3(a) shows the QLCA mode dispersions for the two modes superimposed on the longitudinal fluctuation spectrum, while Fig. 3(b) shows the same curves superimposed on the transverse fluctuation spectrum. The higher (lower) frequency curve in each figure corresponds reasonably well to the longitudinal (transverse) modes obtained from the MD simulations for $ka \lesssim 3$.

Beyond this value of ka (where the two curves nearly touch), the polarization of the modes change so that the lower (upper) curve corresponds to the longitudinal (transverse) mode, which again agrees reasonably well with the spectra obtained from MD simulations.

The eigenvectors (obtained by diagonalizing the dynamical matrix $C_{\mu\nu}$) determine the polarization (i.e., the direction of the particle displacement, or electric field, relative to the direction of propagation) of the modes. In general, the polarization of the modes are mixed, but the respective longitudinal and transverse polarizations prevail for small k [20,21]. The

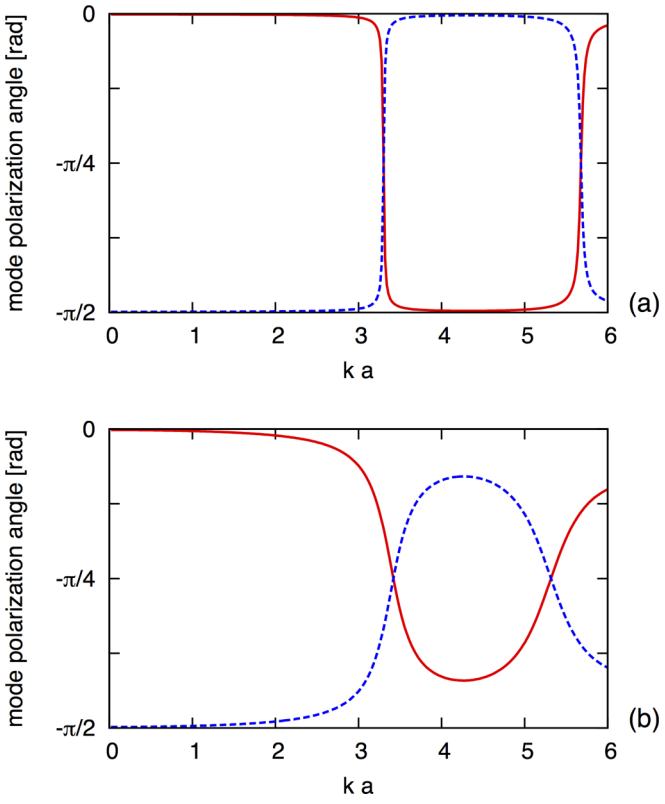

FIG. 4. (Color online) Polarization angles of the two QLCA eigenmodes obtained from (7). Solid (red) curve corresponds to the higher frequency mode, while dashed (blue) curve corresponds to the lower frequency mode. Parameters are $\Gamma = 25$ and $\bar{\kappa} = 1$, with (a) $\eta = 0$, (b) $\alpha = 60^\circ$, $\eta = 0.5$, and $\chi = 30^\circ$.

polarization angle, which is the angle between the normal mode eigenvectors and the wave vector $\mathbf{k}$, depends on the wave number k, the propagation angle χ and also the anisotropy of the system which is characterized to some extent by the value of η. Figure 4(a) shows the polarization angles of the two modes in an isotropic Yukawa system with $\Gamma = 25$ and $\bar{\kappa} = 1$. As can be seen, for $ka \lesssim 3$ the higher frequency mode (denoted by the red solid curve) is longitudinal, while the lower frequency mode (denoted by the blue dashed curve) is transverse. For larger k, however, the mode polarization changes. Near the cross-over point of the two curves (i.e., see Fig. 3) the mode polarization changes from almost pure longitudinal to pure transverse and vice-versa. On the other hand, when the system becomes anisotropic with finite η, the mode polarizations are in general more mixed as a function of k, as can be seen in Fig. 4(b).

Figure 5 illustrates how the magnetic dipole-dipole interaction in a system with finite η modifies the dispersion relations of the modes. Here $\Gamma = 25, \bar{\kappa} = 1$, and $\alpha = 60^\circ$. The top panel considers a case with lower $\eta = 0.2$ while the bottom panel considers a case with larger $\eta = 1$. The columns correspond to wave propagation angles of $\chi = 0^\circ$ (i.e., propagation along the projection of $\mathbf{M}$ in the dust layer), $\chi = 30^\circ$, and $\chi = 90^\circ$ (propagation perpendicular to the projection of $\mathbf{M}$ in the layer). The two modes obtained from the QLCA theory given by (7) with (11) are shown as solid curves, which are superimposed on the longitudinal fluctuation spectra generated by the MD simulations. As can be seen, there is very good agreement between the higher frequency QLCA curves and the longitudinal spectra. One can observe the formation of a deep minimum in the longitudinal mode around $ka = 4$, whose depth is consistently underestimated by the QLCA theory: both the appearance of the minimum and the inadequacy of the QLCA for its description seem to be a universal feature of strongly coupled liquid systems (see Ref. [22]).

There are several physical effects that can be seen in Fig. 5. First, the wave dispersion relations clearly depend on the angle of propagation. Second, for fixed angle of propagation χ, both the sound speed at small k and the maximum frequency of the higher frequency mode increase as η increases. Physically, this reflects the fact that the magnitude of the total repulsive interaction potential increases as η increases, so the mode becomes harder. A third effect is that for fixed η in the larger $\eta = 1$ case, the maximum frequency and the sound velocity of the longitudinal mode appears to decrease as χ increases. On the contrary, the transverse sound velocity increases with χ. This can perhaps be explained by the following observation. As η increases, the particle spacing increases in the y direction owing to the enhanced repulsive interaction in this direction. However, because the areal density is constant, the particles rearrange and the spacings decrease in the x direction, as discussed in relation to Fig. 2. For some parameters (e.g., the $\eta = 0.2$ case in Fig. 5), the total repulsive interaction in the x direction can be comparable to that in the y direction, so there is relatively little variation of the dispersion curve with χ. However, for larger η (e.g., the $\eta = 1$ case in Fig. 5) the total repulsive interaction is substantially larger in the x direction owing to the decreased particle spacing in this direction. This can be roughly quantified by considering the location of the peaks in $g(\bar{r})$ for this set of parameters shown

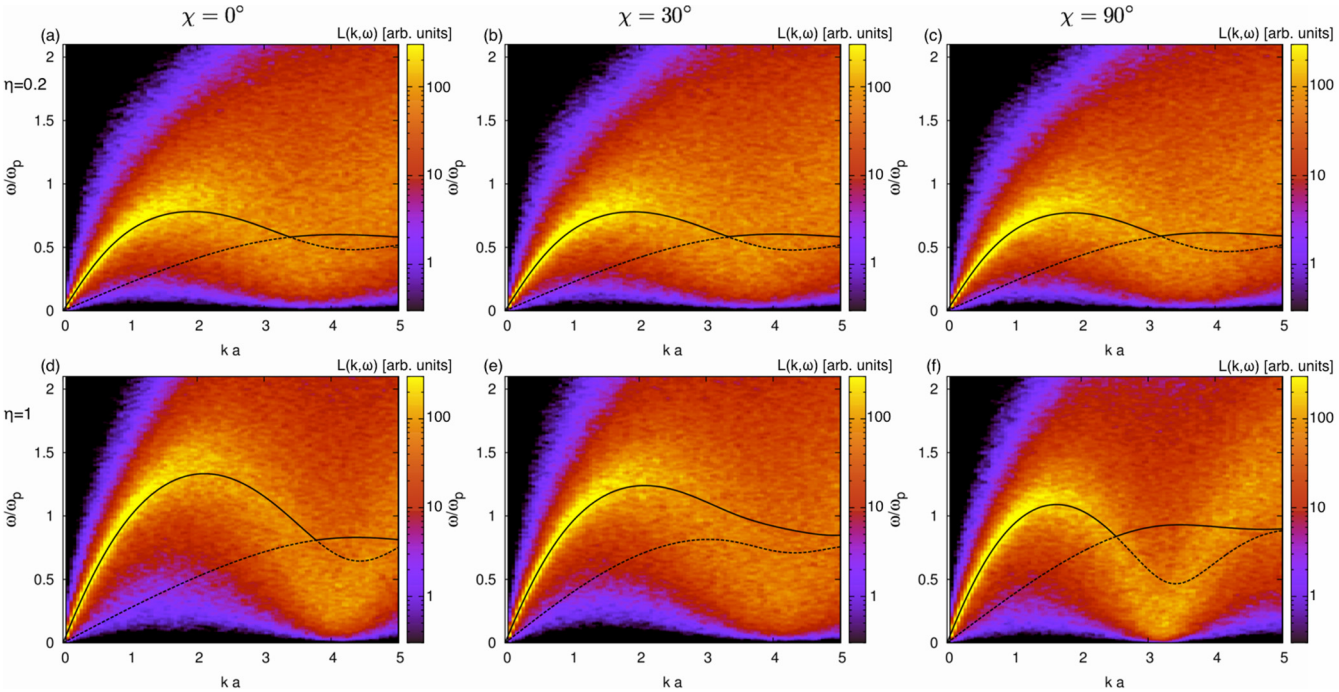

FIG. 5. (Color online) The color maps are the longitudinal fluctuation spectra generated by the simulations. Parameters are $\Gamma = 25$, $\bar{\kappa} = 1$, and $\alpha = 60^\circ$, with the values of η and χ shown in the figure. The solid and dashed curves are the QLCA wave dispersion relations for the two modes obtained from Eq. (7) as a function of ka for these parameters.

in Fig. 2(c). In the x direction, the first peak occurs at $\bar{x} \sim 1.5$, while in the y direction the first peak occurs at $\bar{y} \sim 2$. Thus the softness of the force is compensated by reduced spacing in the x direction and increased spacing in the y direction. Then the second derivative of the interaction potential, which goes roughly like $1/r$ times the force, will be larger in the x direction than in the y direction. Thus the restoring force acting on an oscillating particle for the longitudinal mode, which is proportional to the second derivative of $\phi_{\rm Tot}$ along the direction of propagation, is larger for propagation along the x direction [shown in Fig. 5(d)] relative to that for propagation along the y direction [shown in Fig. 5(f)]. At the same time, the restoring force acting on an oscillating particle for the transverse mode, which is proportional to the second derivative of $\phi_{\rm Tot}$ in the direction perpendicular to the propagation direction, will be larger for propagation along the y direction (also shown in Fig. 6).

Figure 6 shows the same QLCA curves as in Fig. 5, superimposed on the transverse fluctuation spectra generated by the simulations. It can be seen that there is reasonable agreement between the lower frequency QLCA curves and the transverse fluctuation spectra, although the QLCA curves are somewhat higher. Note, however, that the cutoff in the transverse mode at small k is not included in the present QLCA theory (see, e.g., Refs. [15,17,23–25]).

The variation of the sound speeds of the two QLCA modes at small k as a function of propagation angle χ can be seen in Fig. 7. The sound speeds were obtained from Eq. (7) using (11) with the exponential function expanded in a Taylor series. Here $\Gamma = 100$ and $\bar{\kappa} = 1$. Figure 7(a) shows that the sound speeds are isotropic as expected when $\eta = 0$. It can be seen from Fig. 7(b), which is for a case with $\alpha = 60^\circ$ and $\eta = 0.5$, that both sound speeds increase as η increases. In this case, the sound speed of the longitudinal mode exhibits little anisotropy, presumably because the magnitude of the total interaction potential does not vary much with polar angle. However, the sound speed of the transverse mode, which is purely a correlational effect, shows more anisotropy.

V. POSSIBLE EXPERIMENTAL PARAMETERS

To aid in the design of a possible experiment to investigate the wave behavior discussed in this paper, we explore a range of possible parameters for nominal values of Γ, $\bar{\kappa}$ and η discussed in Sec. III. We have used the quantity η as a figure-of-merit to characterize the relative strength of the magnetic dipole-dipole to electrostatic interaction between neighboring grains. For a spherical grain of radius R and magnetic permeability μ, its induced magnetic dipole moment can be expressed as [5]

$$M = R^3\left(\frac{\mu - 1}{\mu + 2}\right)B. \tag{12}$$

The grain charge is given by $Q = R|\phi_s|$ where ϕ_s is the grain surface potential. Thus we have that

$$\eta = \frac{M}{Q\lambda_D} \sim 0.03\,\frac{R^2(\mu\text{m})B(G)}{|\phi_s(V)|\lambda_D(\mu\text{m})}\left(\frac{\mu - 1}{\mu + 2}\right). \tag{13}$$

In the following, we consider possible parameters for systems with $\Gamma = 100$, $\bar{\kappa} = 1$, and $\eta = 0.5$.

We first consider a thermal plasma, with low electron temperature $T_e \sim 0.2$ eV comparable to the ion temperature T_i. Because the dust surface potential would be smaller than in an rf or dc discharge with much larger T_e, we expect that a correspondingly smaller magnetic field would be required

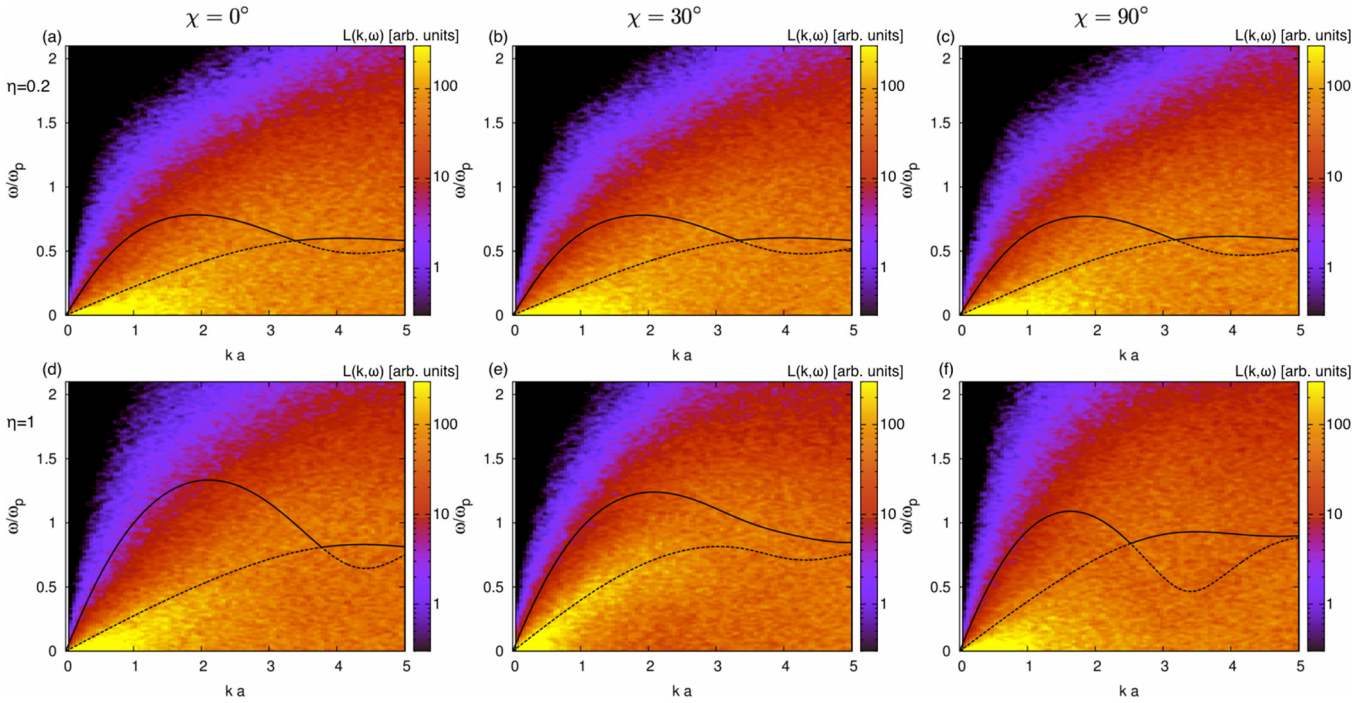

FIG. 6. (Color online) The color maps are the transverse fluctuation spectra generated by the simulations. Parameters are the same as in Fig. 5. The solid and dashed curves are the QLCA wave dispersion relations for the two modes obtained from Eq. (7) as a function of ka for these parameters.

to attain substantial η. Assuming an (argon) ion density $n_i \sim 4 \times 10^8$ cm^{-3}, the linearized Debye length is given by $\lambda_D \sim 0.012$ cm. If we assume that $\mu \sim 4$, $R \sim 5$ μm, and $|\phi_s| \sim 0.5$ V, we obtain $\eta \sim 0.5$ for $B \sim 100$ G. In order to have $\bar{\kappa} = 1$, we require that $a = \lambda_D$, which implies that $n = 1/\pi a^2 \sim 2.2 \times 10^3$ cm^{-2}. The grain coupling parameter requires an estimate of the grain charge and thermal energy. Using $Q_d = R\phi_s = -Z_d e$ we have that the grain charge state $Z_d \sim 2100$. Thus $\Gamma = 100$ implies that T_d should be about 0.5 eV (i.e., the dust thermal speed is about 0.3 mm/s, assuming the dust mass density is about 2 g/cm^3, so the dust mass m_d is $\sim 6.3 \times 10^{14}$ times the proton mass). For these parameters, the dust plasma frequency $\omega_p \sim 34$ rad/s, which implies that the neutral gas pressure should be $\lesssim 2$ Pa in order for the dust-neutral collision frequency, $\nu_{dn} \sim \delta(8\sqrt{2\pi}/3)R^2 n_n v_n m_n/m_d$, to be $\ll \omega_p$ (here n_n, v_n, and m_n are the neutral density, thermal speed, and mass, respectively, and δ ranges from about 1.2–1.4 [26]). Owing to the relatively small charge-to-mass ratio of the grains, however, the electric field E_0 required to levitate the dust grains in the plasma sheath via the electrostatic force QE_0 could be very large for a terrestrial experiment, so this set of parameters might be more relevant for a possible microgravity experiment. We note, however, that dusty plasma experiments in microgravity have generally produced three-dimensional dust clouds in rf or dc plasmas (e.g., [27,28]), so its unclear if dust monolayers could be generated in microgravity.

Next we consider a low-temperature rf or dc discharge type plasma with $T_e \sim 2$ eV, $T_i \sim 0.025$ eV, and (argon) ion density $n_i \sim 1 \times 10^9$ cm^{-3}. We assume the dust layer lies in or near the plasma sheath and that the ions come in to the sheath with an energy $\sim T_e$, so that the Debye length can be estimated using the electron temperature to be about $\lambda_D \sim 0.03$ cm. Requiring that $\bar{\kappa} = 1$ implies that the areal density of the dust is $n \sim 3.5 \times 10^2$ cm^{-2}. We again assume the grains have radius $R \sim 5$ μm, and taking $|\phi_s| \sim 5$, we obtain a dust charge state of $Z_d \sim 1.7 \times 10^4$. Again assuming that $\mu \sim 4$, we find from (13) that a magnetic field of strength of about $B \sim 2000$ G would be needed in order for $\eta = 0.5$. To have the quantity $\Gamma = 100$ would imply a dust thermal energy of about 14 eV (i.e., a dust thermal speed of about 0.3 cm/s, assuming the dust mass density is ~ 2 g/cm^3). With these parameters, one might consider a terrestrial experiment, but the sheath electric field needed to levitate the grains would be of the order of about 30–40 V/cm. The dust plasma frequency for these parameters would be $\omega_p \sim 70$ rad/s, so that the neutral gas pressure should be $\lesssim 4$ Pa in order that $\nu_{dn} \ll \omega_p$.

The presence of an external magnetic field can also have physical effects on the background plasma that can affect the dust. The magnetic field can affect the ion and electrons, which in turn can affect dust charging (e.g., [29,30]), Debye shielding of the grains (e.g., [31]) and ion drag or wind forces acting on the dust arising from ion flows perpendicular to $\mathbf{B}$. If the ions are magnetized there could be ion flows due to $\mathbf{E} \times \mathbf{B}$ or diamagnetic drifts that lead to ion drag forces on the dust (see, e.g., Refs. [32,33]). For the thermal plasma parameters discussed above, the ion Hall parameter β_i, which is the ratio of the ion gyrofrequency to the ion collision frequency, would be about $\beta_i \sim 0.1$ at 2 Pa, so the ions would be weakly magnetized. On the other hand, the ion Hall parameter for the rf or dc discharge parameters discussed above would be on the order of $\beta_i \sim 2$ at 4 Pa, so the ions would be strongly magnetized. Although the discussion of experimental

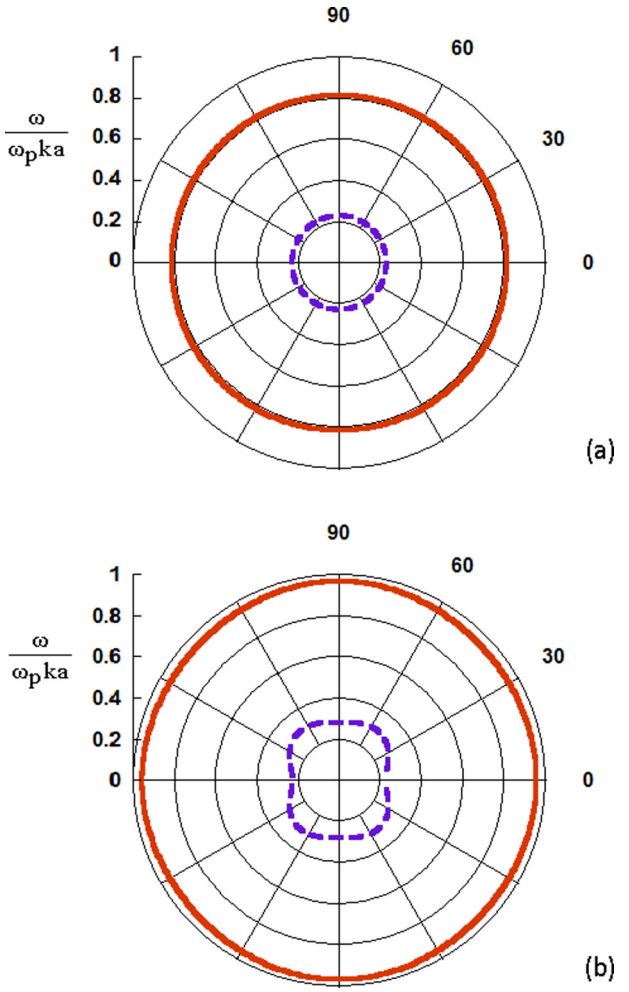

FIG. 7. (Color online) Longitudinal (red, solid curve) and transverse (purple, dashed curve) sound speeds as a function of propagation angle χ obtained from the QLCA expression (7) using (11) and expanding the exponential function for small k. Parameters are $\bar{\kappa} = 1$, with (a) $\Gamma = 100$ and $\eta = 0$, (b) $\alpha = 60^\circ$, $\Gamma = 100$, and $\eta = 0.5$.

challenges is beyond the scope of this paper, we note that there would be an enhanced viscosity between the dust owing to the repulsive magnetic dipole-dipole interaction.

VI. SUMMARY

The dispersion relations of dust waves in the strongly coupled liquid phase of a 2D system of dust grains interacting via both Yukawa and dipole interactions were investigated. The model system comprises a layer of charged superparamagnetic grains in a plasma in an external, uniform magnetic field **B** whose magnitude and direction can be varied. Because the induced magnetic dipole moments of the grains lie along **B**, the interaction between the grains becomes anisotropic as **B** is tilted with respect to the layer. The calculation in this paper is confined to angles between **B** and the layer which are above a threshold angle, where the interaction remains repulsive in the dust layer and generates a stable equilibrium (i.e., with no agglomeration effects).

The theoretical approach uses a reformulated quasilocalized charge approximation that can treat dipole interactions: it requires input of the equilibrium pair correlation functions that are obtained from MD simulations. The QLCA dispersion relations show reasonable agreement with the dispersion relations obtained from the fluctuation spectra generated by the MD simulations. The mode dispersion relations depend on the relative strengths of the Yukawa and dipole interactions and the direction of wave propagation in the plane. In general, the sound speeds of the modes increase as the relative strength of the magnetic dipole-dipole to Yukawa interaction, characterized by the quantity η, increases. There may be possible experimental parameter regimes with moderate magnetic field strengths where such effects could be observed.

ACKNOWLEDGMENTS

M.R. would like to thank Robert An for assistance with numerical computation for Fig. 7. This work was partially supported by NSF Grants No. PHY 0715227, No. PHY 0903808, and No. PHY 1201978, NASA Grant No. NNX10AR54G, NASA/JPL subcontract RSA 1472388, and Hungarian Grants No. OTKA-K-105476 and No. NN-103150.

APPENDIX: ELEMENTS OF DYNAMICAL MATRIX

We give explicitly the elements of the dynamical matrix in the model geometry used in this paper.

$$C_{\mu\nu} = \frac{\omega_p^2}{2\pi}\int d\theta \frac{d\bar{r}}{\bar{r}^2} g(\bar{r},\theta)[\exp(i\bar{k}\bar{r}\cos(\chi-\theta)) - 1]\Phi_{\mu\nu}.$$

Here

$$\Phi_{xx} = \exp(-\bar{\kappa}\bar{r})[(1+\bar{\kappa}\bar{r})(1-3\cos^2\theta) - \cos^2\theta\bar{\kappa}^2\bar{r}^2] + \frac{3\eta^2}{\bar{\kappa}^2\bar{r}^2}[1-5\cos^2\theta+\cos^2\alpha(2-25\cos^2\theta+35\cos^4\theta)],$$

$$\Phi_{yy} = \exp(-\bar{\kappa}\bar{r})[(1+\bar{\kappa}\bar{r})(1-3\sin^2\theta) - \sin^2\theta\bar{\kappa}^2\bar{r}^2] + \frac{3\eta^2}{\bar{\kappa}^2\bar{r}^2}[1-5\sin^2\theta-\cos^2\alpha\cos^2\theta(5-35\sin^2\theta)],$$

$$\Phi_{xy} = \Phi_{yx} = \exp(-\bar{\kappa}\bar{r})[(1+\bar{\kappa}\bar{r})(-3\cos\theta\sin\theta) - \cos\theta\sin\theta\,\bar{\kappa}^2\bar{r}^2] + \frac{3\eta^2}{\bar{\kappa}^2\bar{r}^2} \times [\cos\theta\sin\theta(-5-\cos^2\alpha(10-35\cos^2\theta)],$$

$$\Phi_{zz} = \exp(-\bar{\kappa}\bar{r})(1+\bar{\kappa}\bar{r}) + \frac{3\eta^2}{\bar{\kappa}^2\bar{r}^2}[1-5\cos^2\alpha\cos^2\theta+2\sin^2\alpha],$$

$$\Phi_{zx} = \Phi_{xz} = \frac{3\eta^2}{\bar{\kappa}^2\bar{r}^2}[\sin\alpha\cos\alpha(2-10\cos^2\theta)],$$

$$\Phi_{zy} = \Phi_{yz} = \frac{3\eta^2}{\bar{\kappa}^2\bar{r}^2}[-10\sin\alpha\cos\alpha\sin\theta\cos\theta].$$

[1] M. Bonitz, C. Henning, and D. Block, Rep. Prog. Phys. **73**, 066501 (2010).
[2] P. K. Shukla and B. Eliasson, Rev. Mod. Phys. **81**, 25 (2009).
[3] V. E. Fortov, A. V. Ivlev, S. A. Khrapak, A. G. Khrapak, and G. E. Morfill, Phys. Rep. **421**, 1 (2005).
[4] D. Samsonov, S. Zhdanov, G. Morfill, and V. Steinberg, New J. Phys. **5**, 24 (2003).
[5] V. V. Yaroshenko, G. E. Morfill, D. Samsonov, and S. V. Vladimirov, IEEE Trans. Plasma Sci. **32**, 675 (2004).
[6] P. Hartmann, M. Rosenberg, G. J. Kalman, and Z. Donko, Phys. Rev. E **84**, 016409 (2011).
[7] J. D. Feldmann, G. J. Kalman, P. Hartmann, and M. Rosenberg, Phys. Rev. Lett. **100**, 085001 (2008).
[8] A. V. Ivlev, G. E. Morfill, H. M. Thomas, C. Rath *et al*., Phys. Rev. Lett. **100**, 095003 (2008).
[9] A. V. Ivlev, P. C. Brandt, G. E. Morfill, C. Rath *et al*., IEEE Trans. Plasma Sci. **38**, 733 (2010).
[10] V. V. Yaroshenko and G. E. Morfill, New J. Phys. **7**, 207 (2005).
[11] K. I. Golden, G. J. Kalman, Z. Donko, and P. Hartmann, Phys. Rev. B **78**, 045304 (2008); **78**, 239905(E) (2008).
[12] K. I. Golden, G. J. Kalman, Z. Donko, and P. Hartmann, J. Phys. A: Math. Theor. **42**, 214017 (2009).
[13] K. I. Golden, G. J. Kalman, P. Hartmann, and Z. Donko, Phys. Rev. E **82**, 036402 (2010).
[14] N. Hoffman, C. N. Likos, and H. Lowen, Mol. Phys. **105**, 1849 (2007).
[15] Z. Donko, G. J. Kalman, and P. Hartmann, J. Phys.: Condens. Matter **20**, 413101 (2008).
[16] T. Ott, D. A. Baiko, H. Kahlert, and M. Bonitz, Phys. Rev. E **87**, 043102 (2013).
[17] K. I. Golden and G. J. Kalman, Phys. Plasmas **7**, 14 (2000).
[18] N. W. Ashcroft and N. D. Mermin, *Solid State Physics* (Holt, Rinehart and Winston, New York, 1976).
[19] J. P. Hansen, I. R. McDonald, and E. L. Pollock, Phys. Rev. A **11**, 1025 (1975).
[20] P. Hartmann, Z. Donko, G. J. Kalman, S. Kyrkos, M. Rosenberg, and P. M. Bakshi, IEEE Trans. Plasma Sci. **35**, 337 (2007).
[21] S. Zhdanov, S. Nunomura, D. Samsonov, and G. Morfill, Phys. Rev. E **68**, 035401 (2003).
[22] G. J. Kalman, S. Kyrkos, K. I. Golden, P. Hartmann, and Z. Donko, Contrib. Plasma Phys. **52**, 219 (2012).
[23] M. S. Murillo, Phys. Rev. Lett. **85**, 2514 (2000).
[24] S. Hamaguchi and H. Ohta, Phys. Scr. **T89**, 127 (2001).
[25] J. Goree, Z. Donko, and P. Hartmann, Phys. Rev. E **85**, 066401 (2012).
[26] S. A. Khrapak, A. V. Ivlev, and G. E. Morfill, Phys. Rev. E **70**, 056405 (2004).
[27] O. Arp, J. Goree, and A. Piel, Phys. Rev. E **85**, 046409 (2012).
[28] V. Fortov, G. Morfill, O. Petrov, M. Thoma *et al*., Plasma Phys. Control. Fusion **47**, B537 (2005)..
[29] J. S. Chang and K. Spariosu, J. Phys. Soc. Jpn. **62**, 97 (1993).
[30] V. N. Tsytovich, N. Sato, and G. E. Morfill, New J. Phys. **5**, 43 (2003).
[31] M. Salimullah, P. K. Shukla, M. Nambu, H. Nitta, O. Isihara, and A. M. Riswan, Phys. Plasmas **10**, 3047 (2003).
[32] P. K. Kaw, K. Nishikawa, and N. Sato, Phys. Plasmas **9**, 387 (2002).
[33] I. Pilch, T. Reichstein, and A. Piel, Phys. Plasmas **15**, 103706 (2008).